Simulation of Anti-Compton Shield Augmentation to the Lundium Decay Station Using `Geant4`

Daesung Cho
Supervised by Luis Sarmiento Pico
Co-supervised by Daniel Cox

Bachelor's Thesis
Division of Nuclear Physics, Lund University
Project Duration: January - May 2019

LUND
UNIVERSITY

Abstract

The Lundium decay station improves on the existing TASISpec spectrometer used to investigate the nuclear structure of superheavy nuclei by photon- and charged particle-spectroscopy. This thesis aims to explore the potential benefits of the future Lundium station with the augmentation of anti-Compton shields composed by a set of BGO scintillator bars. The effects of anti-Compton shields was investigated through a simulation toolkit, `Geant4`, developed by CERN. The Lundium station augmented by the anti-Compton shields was constructed in the simulation framework, then simulations of two point-like isotropic sources, 661.7 keV and Eu-152, located at the Lundium focal plane were done. A beam-spot like Cs-137 was also simulated. The data was sorted and analyzed considering the effects of Compton scattering and the geometry of the setup. The response of Lundium and Lundium with anti-Compton shields augmentation was compared using the 661.7 keV gamma source. The effects of a more realistic situation were examined with the Cs-137 distribution, and the detector response of high energy gamma rays were explored using Eu-152. The anti-Compton shield augmentation yielded peak-to-background percentage increase of roughly 9% with comparable results in the more realistic simulation with Cs-137 distribution. The use of anti-Compton shields with multiple energies of photons was also successful in increasing the relative peak intensities.

List of Acronyms

Geant4	GEometry ANd Tracking 4
BGO	Bismuth Germanate
SHE	SuperHeavy Elements
HPGe	High Purity Germanium Detector
ACS	Anti-Compton Shield
TASCA	TransActinide Separator and Chemistry Apparatus
TASISpec	TAsca in Small Image mode Spectroscopy
PMT	Photomultiplier Tube
DSSSD	Double Sided Silicon Strip Detector
Go4	GSI Object Oriented On-line Off-line system

Contents

1 Introduction

Following a series of discoveries of naturally-occurring elements and efforts to synthesize new elements, discovering new heavier elements becomes increasingly difficult due to increased instability from the number of protons causing spontaneous fission and alpha decay [1]. New elements such as element 112 to 118 that were discovered in the past decades are well into the territory of SuperHeavy Elements (SHE) which are defined as consisting of more than 103 protons. While the widely used liquid-drop model of nuclei does not allow for elements with significant stability in the superheavy region, the nuclear shell model predicts a region in the nuclide chart where there is increase in stability due to filled nuclear shells around $Z = 114$ and $N = 184$ or $Z = 120$ and $N = 172$ [2, 3]. Current research efforts are working to understand the effects of the magic numbers to the nuclear structure in this region, referred to as the "Island of Stability".

Elements around the "Island" are generally synthesized by accelerating medium-sized ions such as Ca-48 and Ti-50 into heavier actinide nuclei such as americium, berkelium, and curium [4, 5]. The synthesized nuclei are detected by their characteristic alpha-decay chains. Each step in the alpha-decay chain can result in an excited state in the daughter nucleus which consequently emits photons either by γ decay or X-rays after internal conversion [4, 6]. The energies of the emitted photons are characteristic to the isotopes of the daughter nuclei, allowing for identification and confirmation of the predicted decay chains and consequently the synthesized SHE [4].

Detecting and characterizing these elements pose a challenge due to the difficulties synthesizing them from the small fusion cross section and the unavailability of costly target and beam materials. Thus, high detection efficiency is required to study these rare elements. The Nuclear Structure Group in Lund has used the TAsca in Small Image mode Spectroscopy (TASISpec) decay station to fingerprint and characterize SHE in the past [6]. TASISpec accomplishes this through spectroscopy of α particles and photons by the use of silicon and germanium semiconductor detectors [6]. An improved decay station to TASISpec has been envisioned, referred to as "Lundium," aiming to increase detection efficiency by increasing angular coverage of the High Purity Germanium Detector (HPGe) detectors, optimizing shielding, and decreasing the distance to the TransActinide Separator and Chemistry Apparatus (TASCA) focal plane [7].

One of the changes from TASISpec to Lundium is the HPGe detectors. The new detectors, referred to as COMPEX and described in Section 3.2, are designed to be more efficient and obtain higher resolution at low energies than those used in TASISpec such as the VEGA, SHIP, and EUROBALL Ge clover and cluster detectors [6, 8]. The COMPEX detectors allows for better efficiency through a wider angular coverage due to their shapes and proximity to the silicon detectors. The benefits of COMPEX over VEGA and SHIP have been simulated and characterized [7].

A possible augmentation to Lundium as currently envisioned is configurations of Anti-Compton Shield (ACS)'s to be used in conjunction with COMPEX. Compton scattering in detectors can cause distribution of the photon energy to different particles, forming a continuous Compton background, and can also leave a portion of the energy unregistered in cases of escaped photons and electrons [9]. These effects need to be considered in optimizing shielding, and the ACS's are placed to account for incomplete detections by measuring escaping photons caused by Compton scattering as well as background effects [7]. This thesis work aims to examine the possible benefits of ACS augmentation to the Lundium setup by the use of the `GEometry ANd Tracking 4 (Geant4)` simulation

toolkit.

`Geant4` is a Monte Carlo simulation toolkit developed at CERN for the interaction of particles through matter [10]. Written in C++, it provides a framework for a user to create objects and physical processes which interact with generated particles given certain user-defined parameters that include physical phenomena. `Geant4` is used to validate experimental setup and data and is currently maintained with active development. `Geant4` simulations have been successfully used in the SHE region for setups like TASISpec to shed light in the data interpretation of SHE research [8, 11, 12].

The following section describes the physics of photon interactions with matter. The detector types used in the Lundium setup are described in Section 3 followed by the description of the decay station setups in Section 4. Descriptions and details of the simulation environment `Geant4` are given in Section 5. Then the methods of data analysis are described in Section 6, and the results are presented in Section 7. The conclusion and outlook is presented in the final section.

2 Gamma Ray Interactions

Photons can interact with matter differently depending on their energy. The three main ways that a photon interacts with matter in the relevant energy range are photoelectric absorption, pair production, and Compton scattering. Photo-nuclear reactions can occur at higher energies, but those energies are beyond the scope of this work. Photoelectric absorption refers to a photon being absorbed by an electron, causing it to ionize, and it is significantly more probable for photons with low energy ($\sim$ 100 keV) [13]. Pair production is the creation of an electron-positron pair from a photon and can only exist for high energy photons with energies greater than 1.022 MeV [13]. Contrary to the other two interactions, Compton scattering can occur over a wide range of energies [13].

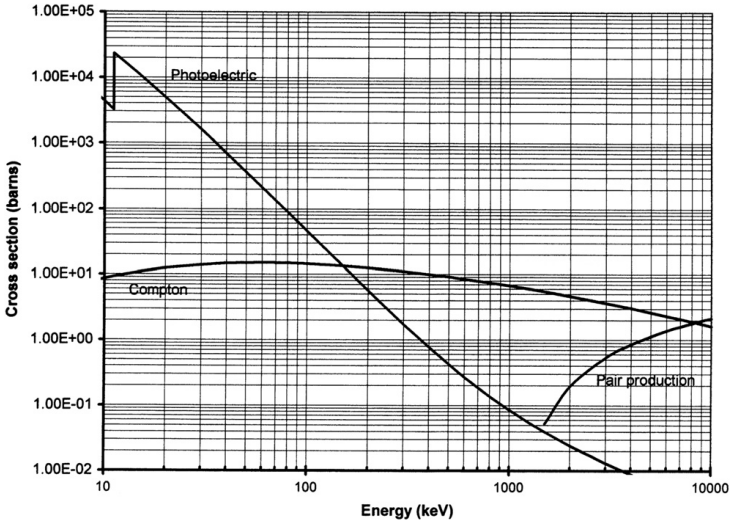

Figure 1: Cross-section of γ interactions in Ge detectors [14]

Figure 1 shows the cross-sections of the three previously mentioned photon interactions in a germanium detector. As shown in the figure, pair production only occurs above 1.022 MeV with increasing cross-section with higher energies while Compton scattering has a consistent cross-section across the energy range shown in the plot.

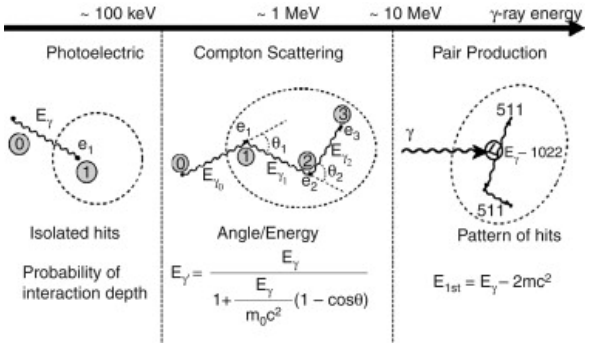

Figure 2: Interactions of gamma rays in a detector over a energy range [9]

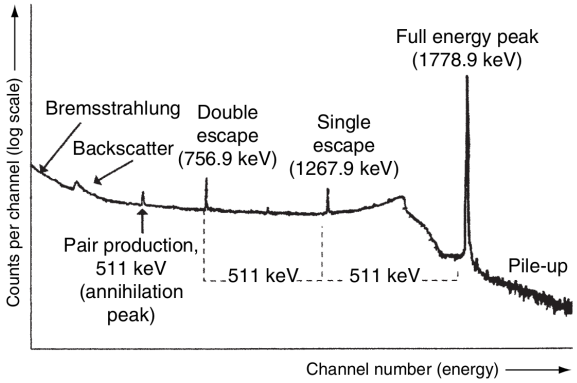

Figure 3: Typical gamma spectrum of ^{28}Al as detected by a germanium detector [9]

In detecting γ rays, registration of the entire γ energy leads to a full-energy peak in the gamma spectrum, also denoted photopeak. Through the different photon interactions, the detected energies can differ, leading to typical characteristics of gamma spectroscopy such as the Compton continuum, single- and double-escape peaks, and the Compton edge [14]. These characteristics are shown in Figure 3, and the formation of them is discussed below with each interaction.

2.1 Photoelectric Absorption

Photoelectric absorption leads to an electron ejected from an atom, leaving the atom in an excited state [9]. The atom is left with excess energy which is also the binding energy of the ejected electron, E_b, as used in Equation 1, where E_e is the kinetic energy of the ejected electron and E_γ the energy of the incoming photon [9]. After the ejection of the electron, the excited atom can lose energy by emission of X-ray following deexcitation of a higher shell electron into the hole left by the ejected electron [9]. The energies of the X-ray emissions are characteristic to each element, providing a useful indicator in fingerprinting elements [9].

$$E_e = E_\gamma - E_b \tag{1}$$

2.2 Compton Scattering

Compton scattering is the interaction between a photon and a charged particle, usually an electron, resulting in scattering of the photon and the particle itself [15]. This process leads to transfer of momentum to the charged particle, leaving the photon with less energy. The reduced photon energy, shown in Equation 2, depends on the initial photon energy and the scattered angle [13]. Addition to the energy of the photon, E_γ, alpha expresses the ratio between the energy of the photon and the electron rest energy, $\alpha = E_\gamma / mc^2$.

$$E'_\gamma = \frac{E_\gamma}{1 + \alpha(1 - \cos\theta)} \tag{2}$$

The cross-section for Compton scattering is dependent on the incident energy of the photon. Figure 4 illustrates the relationship between cross-section of Compton scattering with its scattering angle, ϑ, and energy ratio, α, for a photon incident from the left horizontally in the figure. Photons with low energy such as $\alpha < 0.1$ have a comparable

probability to scatter at various angles while for high energies such as $\alpha = 10$ the cross-section for scattering heavily favors low scattering angles in the incident direction of the photon with almost no probability to scatter in the opposite direction. Backscattering becomes increasingly unlikely for higher energies. A photon may undergo multiple Compton scattering events, losing energy with each interaction. This process in a detector is illustrated in Figure 2.

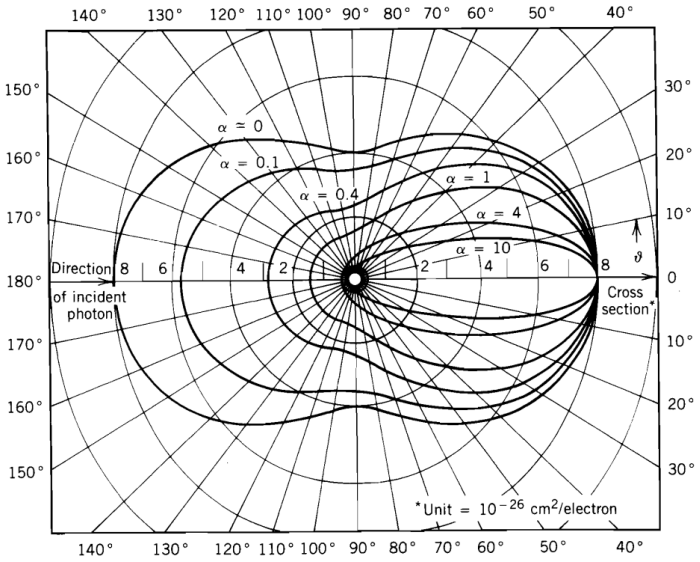

Figure 4: The Compton-scattering angle distribution with cross section for various incident energies [13]

The Klein-Nishina formula, Equation 3, describes the probability for an unpolarized photon to Compton scatter at some angle and energy where r_0 is the classical electron radius, α the energy ratio as in Equation 2, and θ the scattered angle [13].

$$\frac{d\sigma}{d\Omega} = r_0^2 \left[\frac{1}{1+\alpha(1-\cos\theta)}\right]^3 \left[\frac{1+cos\theta}{2}\right] \left[1 + \frac{\alpha^2(1-\cos\theta)^2}{(1+\cos^2\theta)[1+\alpha(1-\cos\theta)]}\right] \tag{3}$$

By integrating the Klein-Nishina formula, the absorption of photons can be found.

$$\sigma = \frac{\pi r_0^2}{\alpha} \left\{ \left[1 - \frac{2(\alpha+1)}{\alpha^2}\right] \ln(2\alpha+1) + \frac{1}{2} + \frac{4}{\alpha} - \frac{1}{2(2\alpha+1)^2} \right\} \tag{4}$$

Since Compton scattering does not decrease the energy of the photons in discrete steps and a photon may undergo multiple scattering events, the scattered photons form a continuous energy spectrum known as the Compton continuum shown as a relatively horizontal curve ranging from 0 to around 1.5 MeV in Figure 3 [14]. The Compton edge is formed if the Compton effect of an incident photon causes it to scatter backwards (180°) and subsequently escapes the detection volume [14]. If a photon enters the detection volume as a result of Compton scattering at 180° from the surrounding materials, the detected photons form a backscatter peak [14]. The Compton edge and the backscatter peak are also shown in Figure 3 with the Compton edge located at around 1.5MeV where the spectrum begin to decline rapidly following the Compton edge. The Compton edge also marks the end of the Compton continuum for a single scattering event as it signifies scattering at 180°while smaller scattering angles are included in the continuum. The

purpose of ACS is to account for the photons scattered from the relevant main detector in a setup (Ge in this case) in order to reduce the intensity of the Compton continuum.

2.3 Pair Production

A photon with a sufficiently high energy can transform into a positron and an electron pair. Since the positron readily annihilates with electrons due to them being antiparticles of each other, initial pair production leads to emission of two 0.511 MeV photons when the resulting positron annihilate with an electron [15].

The photons created from the electron-positron annihilation can escape the detector volume depending on the size of the detector. Single- and double-escape peaks form when one or both of the photons escape from the detection volume, respectively [15]. The single- and double-escape peaks are located 0.511 MeV and 1.022 MeV lower than their respective photopeak. These escape peaks are illustrated in Figure 3 with energy gaps respect to the full energy peak.

3 Detector Types

The Lundium station as such will use two types of semiconductor detectorees, silicon for charged particles and germanium for photons. In this work, new scintillator bars made out of Bismuth Germanate (BGO) will be used.

3.1 Silicon (Si)

In the center of the Lundium station, five silicon detectors form a box with one open side. A Double Sided Silicon Strip Detector (DSSSD) is placed opposite of the open side and four additional DSSSDs are placed upstream from the beam direction to form the other sides of the box. A render of this silicon detector box is shown in Figure 5.

These silicon detectors are used to detect charged particles from possible decays and are effectively transparent to γ radiation due to its thinness [6, 16]. A number of silicon detector varieties exist with different thicknesses. However, the specifications of the silicon detectors are not relevant in the scope of this work.

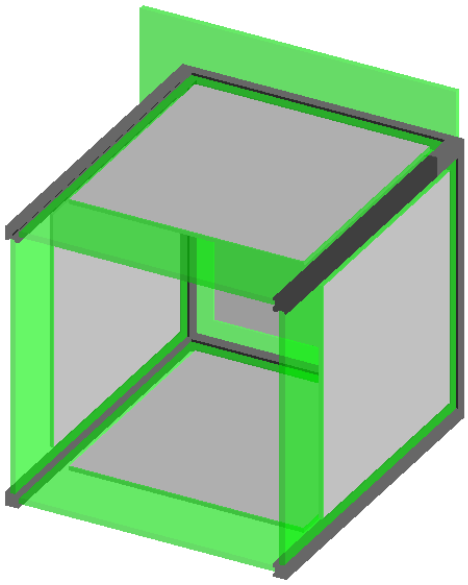

Figure 5: Render of Silicon Detector Box from `Geant4`

3.2 COMPEX (HPGe)

The Lundium setup will use five composite HPGe detectors placed behind each silicon detector. The placements of the COMPEX detectors are shown in a render of the Lundium setup in Figure 8.

Renders of the construction of COMPEX detectors are shown in Figure 6. There are four 5x5x5cm^3 germanium crystals in each COMPEX detector in a 2 by 2 array.

Conventional Ge detectors are cylindrical with coaxial cores that are used to form the electric field. However, the crystals in COMPEX are formed to be as square as possible to be closely packed. Due to physical limitations of fabricating the Ge crystals, the crystals are rounded and tapered on the corners as shown in Figure 6a.

Each of the 4 crystals are individually encapsulated in vacuum in a cubic aluminum casing. Singular encapsulation of the crystals allow for individual maintenance and repair. This is another advantage of COMPEX over other HPGe detectors as this quality makes maintenance easier and increases the lifetime of the detector as a whole.

Figure 6a also displays an orange object rendered behind the crystals. This cylinder is a representation of the copper contact between the HPGe crystals and the consequent cooling and electronics. Since HPGe must be operated at low temperatures ($\sim$ 77K), the copper contact is used to cool down the crystals due to its high conductivity [15]. Further details of the contact are omitted under the assumption that the present detail is sufficient to simulate the effects of additional components.

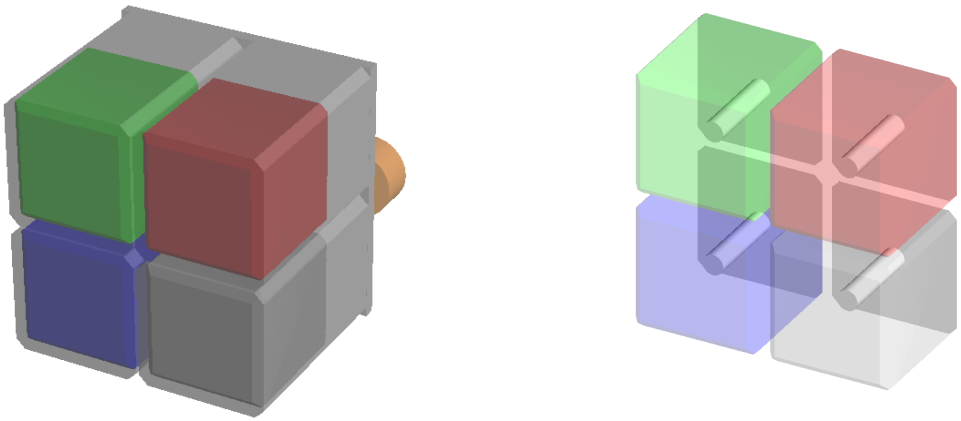

(a) Semi-transparent view of COMPEX illustrating the Ge crystals

(b) COMPEX with increased transparency with cylindrical cavities

Figure 6: Renders of singular COMPEX detectors with different object transparencies

Figure 6b shows transparent Ge crystals to exhibit the cylindrical cavity and the solid back that make up the dead layer. Similar to cylindrical HPGe detectors, these cylindrical cavities present in each crystals are empty volumes where the surface acts as the anode or the cathode for high voltages required to bias the crystals.

3.3 Bismuth Germanate (BGO)

Scintillator detectors generally provide higher efficiency than semiconductor detectors in sacrifice of resolution [9]. This characteristic as well as better time resolution makes them more suitable for use in ACS purposes as it is more important to detect the maximum number of events than to detect them with high energy resolution.

Photons themselves are not directly detected by the scintillator detectors. These detectors function by converting the incoming photons to scintillation photons which are then turned into multiple photoelectrons at the photocathode. These few number of photoelectrons are then multiplied in the Photomultiplier Tube (PMT) to create an amplified signal as current that can be measured [15]. The PMT is not included in this simulated construction of the Lundium setup, but the interface between the BGO's and

their corresponding PMT's are accounted for as visible tapers on the right end of BGO crystal shown in Figure 7b. In addition, this simulation work only accounts for direct energy depositions to the detectors. The simulations of optical photons in the scintillators are not in the scope of this work and is thus omitted.

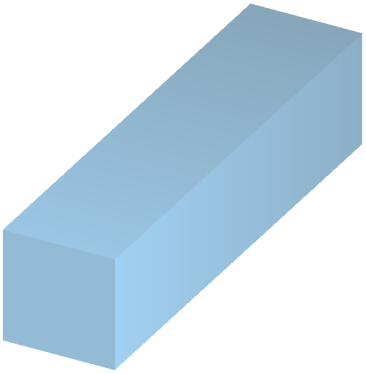

(a) Single BGO bar

(b) Side view, notice the tapered end where the PMT or other readout scheme will be connected

Figure 7: Rendered singular BGO crystal

The performance of scintillator detectors is determined by its density and the atomic numbers of the material [15]. Inorganic scintillators such as BGO are generally preferred for γ-detection for their high Z's and bulk densities as the stopping power and thus the detection efficiency scales with $\sim Z^4$ [15]. Bismuth germanate, $Bi_4Ge_3O_{12}$, has density of 7.13 g/cm^3 with the largest atomic number 83 from bismuth. Due to its high density and atomic number, BGO provides the largest probability for photoelectric absorbtion per unit volume [15].

Figure 7 shows rendered images of BGO crystals from two different angles. The dimensions of the crystals are 19x19x80mm^3 with a 2mm taper on the end. This taper is to account for the optical guide between the BGO and the PMT.

4 Detector Setup

The Lundium decay station is envisioned to be used to characterize and fingerprint SHE through high resolution particle and photon spectroscopy [7, 17]. An upgrade to the currently in use TASISpec, Lundium aims to use new designs including new HPGe detectors, COMPEX, to increase the detection efficiency.

Anti-Compton Shield In the context of γ- & X-ray spectroscopy and detector setups, Compton scattering causes a Compton continuum to form for scattered photons escaping the detection volume, reducing the intensities of desired photopeaks [18]. Scintillator detectors such as NaI(Tl) and BGO, can be placed around the detector to account for these occurrences by observing the escaping photons [18, 19]. These detectors are purposed to act as the ACS in the setup.

The main scope of the thesis work is evaluation of augmenting BGO scintillator detectors around the COMPEX detectors to enhance the Lundium setup. An array of BGO's around a single COMPEX is shown in Figure 9. The placements of the BGO's can be

changed, and in the case of the Lundium set up, they have to be changed to fit the ACS around each COMPEX detector.

4.1 Lundium Decay Station Setup

The Lundium decay station as currently envisioned consists of 5 COMPEX detectors, see Figure 6, surrounding the silicon detector box, Figure 5, on its 4 sides as well as an additional COMPEX at the back. A render of the Lundium station without ACS is shown in Figure 8. The design resembles TASISpec in essence with silicon box at the core surrounded by HPGe detectors but offers much higher detection efficiency through the use of COMPEX detectors which have higher solid angle coverage compared to the VEGA and SHIP clovers used in TASISpec.

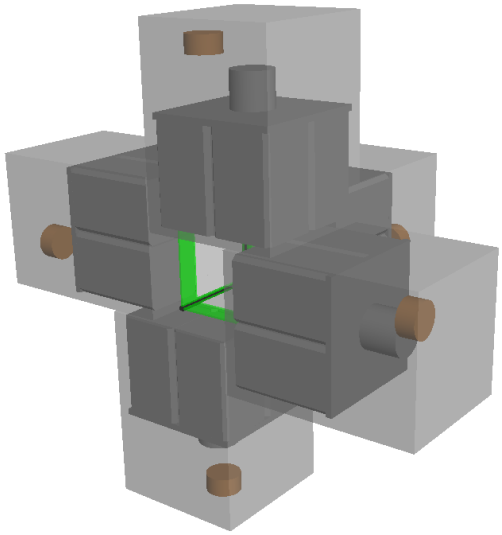

Figure 8: Semitransparent render of the Lundium setup without ACS

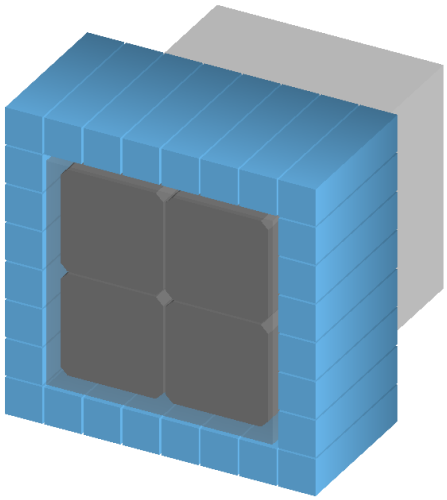

Figure 9: Render of a COMPEX detector with 28 BGO bars to be used as part of Anti-Compton Shield

4.2 Lundium Setup with Anti-Compton Shields

Anti-Compton shields can be used in the Lundium setup through the augmentation of BGO crystals to surround the COMPEX detector as shown in Figure 9. Each COMPEX detector is accompanied by 28 BGO bars which perform as the anti-Compton shields. Addition of BGO bars to each of the COMPEX in Lundium setup completes the ACS implementation, shown in Figure 10. As shown, each COMPEX detector is surrounded by 28 BGO crystals. In order to fit the BGO without overlap, the ring of BGOs was placed 42.5mm from the front of each of the COMPEX detectors except the COMPEX located at the back. The back ACS ring required no offset and is thus placed on the same plane as the front of the COMPEX detector. The lack of offset is clearly visible in the side view in Figure 10.

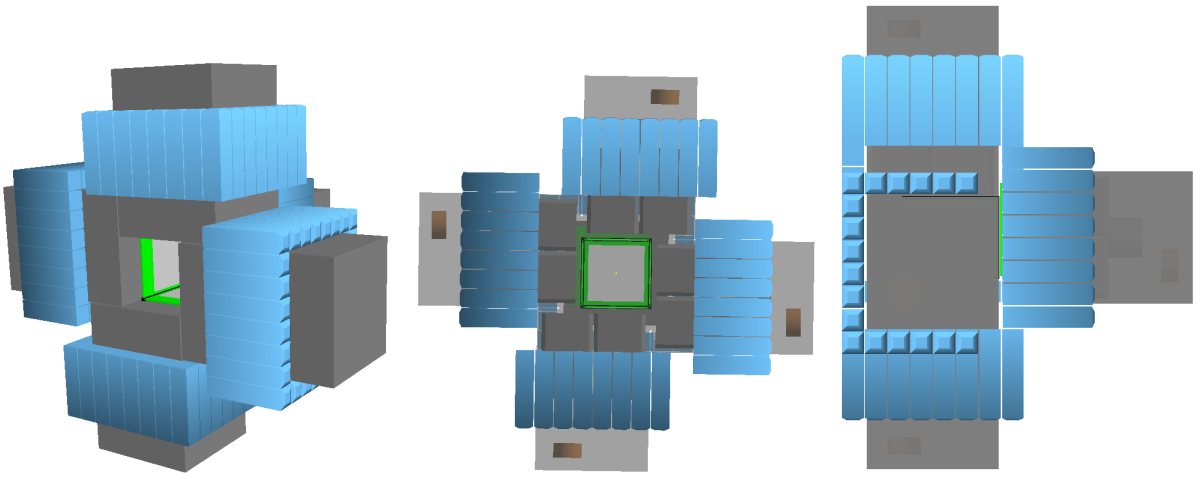

Figure 10: Renderings of Lundium with ACS including front (middle) and side view (right). 10 BGO bars were removed from the render in the side view to exhibit the front plane of the COMPEX located at the back with its BGOs

5 Simulation Using `Geant4`

The detector responses of the setups will be simulated through the simulation toolkit `Geant4`. `Geant4` simulates the transport of particles through matter based on Montel Carlo methods with user definable objects, environments, and physical effects. The Lundium station and the augmented ACS are simulated using `Geant4`. Relevant physics processes are defined, and sources of radiation are placed in order to run the simulation. This thesis work is an extension of the simulation framework constructed by L. G. Sarmiento in previous works involving Lundium as well as other decay stations such as TASISpec [7, 8]. `Geant4` version 10.05 was used for this work.

The following section explains the Monte Carlo method, and the technicalities and specifics of `Geant4` and the simulations are described.

5.1 Monte Carlo Method

Monte Carlo method is a commonly used technique employing random number generation and statistics to solve numerical problems [20]. Monte Carlo method is particularly useful in particle and nuclear physics simulation since many processes are modeled and understood by statistical trend rooting from randomness such as radioactive decay [21]. This property of particle and nuclear physics makes Monte Carlo method a strong foundation to build a comprehensive simulation toolkit such as `Geant4`.

5.2 Design of Simulation

Three classes are required to run simulations in `Geant4`: DetectorConstruction, PhysicsList, and Primary Generator Action. The Detector Construction class defines the spaces, volumes, materials, placements, and other properties of objects that exist in the simulation environment. PhysicsList defines what physical phenomena and interactions are to be included in the simulation. Different physics lists are provided with `Geant4` to be

tailored for the user's needs. Primary Generator Action defines the occurrences of initial physical processes such as a particle beam.

5.2.1 Detector Construction

One of the first steps is to define the simulation environment. For this thesis, the environment was a simple vacuum that encapsulated the entire detector setup. This virtual vacuum allows for omission of aluminum chamber that Lundium must be encased within in real experiments to create a vacuum for the silicon box and the fronts of COMPEX detectors.

In `Geant4`, objects are created in layers that define different properties of the objects. In order to create an object a G4Solid (Geant4Solid; henceforth referred to "Solid") is first created that defines the shape and size of an object. The Solid is then put into a G4LogicalVolume ("LogicalVolume") that defines the material of the Solid and other physical attributes inherent to the object. The object is finally placed into the simulation environment by the G4PhysicalVolume where the position of the object is defined.

Lundium The Lundium station, already existing in `Geant4` environment from L.G. Sarmiento, was created in `Geant4` environment by initializing instances of detector classes and placing them in a modular fashion. Separate LogicalVolume classes defined the COMPEX and the silicon detectors. These classes were instantiated into the world by placing them. The COMPEX detectors were initialized multiple times while rotating the position vector, allowing for the geometry shown in Figure 8. The COMPEX at the rear was instantiated separately.

Lundium with ACS In order to fit the ACS in each COMPEX, a new class was created derived from the existing COMPEX class. The new class included the BGO arrays with a depth parameter to change the position the array in relation to the front of the COMPEX. The new class with COMPEX and ACS was then initialized similarly to the Lundium setup. The appropriate depth was found to eliminate any overlaps and to minimize empty spaces between the shields. The rear COMPEX was instantiated separately from the radial ones in this case as well. The ACS for the rear COMPEX caused no overlap with the rest of the setup when placed at the front in the same plane as the COMPEX. The rendered result of this construction is shown in Figure 10.

5.2.2 PhysicsList

`Geant4` provides predefined physics lists that include core physics mechanics for general and specific use cases. Different physics lists deal with varying ranges of energies and particles that can be chosen by the users to build simulations suited for their purposes.

Regular physics lists such as G4IonPhysics, that include transport of ions were used. To simulate photon interactions and nuclear decays, the following physics lists were additionally used: G4EmLivermorePhysics, G4DecayPhysics, G4RadioactiveDecayPhysics.

5.2.3 Primary Generator Action

The Primary Generator Action class defines what physical processes occurs in the simulation including but not limited to the composition of particles, placement and/or movement

of the particles, and restrictions on the radiation emission. The details of the radiation sources used in this simulations are specified below in Section 7.

5.3 Simulated Data Output

`Geant4` is able to output data in different formats. ROOT format is used to gather data in these simulations due to its capability to store large amounts of data that can be used by the ROOT data analysis framework [22]. `Geant4` recognizes interactions of photons with matter as hits to the objects. From the simulations, the object ID (detector), energy deposited, and time are recorded.

6 Data Analysis

Analysis of the raw data includes sorting the data according to the detectors that the hit registers and their energies as well as filtering the sorted data to account for possible physical occurrences in the simulated environment such as scattered photons and lost energies from escaping particles. Python scripts using ROOT functions were used to analyze the data, and the `GSI Object Oriented On-line Off-line system (Go4)` was used to visualize and further analyze sorted and filtered data.

6.1 Offline Data Sorting

Each hit on an object by a particle in `Geant4` contributes to the object's counts. These objects are assigned IDs in the simulation which need to be identified as detectors by matching the object ID to the corresponding crystal. With the crystals in the setup identified with corresponding IDs, the IDs of the detectors can be found by grouping a range of IDs for COMPEX detectors and finding the corresponding ID range for BGOs. For example, a COMPEX detector is assigned 4 ID numbers, one for each Ge crystal, which are grouped together to be identified as one of the COMPEX detectors. Then a range of 28 IDs are found for the corresponding BGO array where each BGO is assigned one ID. The registered hits to the objects are then sorted for the IDs to be associated to the detectors to complete the data sorting.

6.2 Schemes of Data Filtering

Once that each of the detectors can be identified by their unique ID, the relationships between them regarding physical distance and hence their relevance to nearby detectors are defined in a "distance matrix." For example, a Ge crystal in a COMPEX is assigned distance of 1 to its direct adjacent crystals while 2 is assigned to the crystal diagonal to it. In a similar fashion, distance matrices were created for each crystal, 20 total, that includes its nearby BGO bars. BGO bars directly adjacent to the Ge crystals as well as the BGOs diagonal to the corners are assigned distance 1. The other BGO bars are assigned an arbitrary "far" distance, indicating that they are too far apart to have meaningful interactions with the same photon.

With the sorted data and the distance matrix, the data can be further analyzed to consider different Compton scattering possibilities. The sorted data was filtered into 4 variants: Spectrum, Suppressed, Added back, Added back with suppression.

Spectrum The "Spectrum" filter, written as "Spectrum" to differentiate from the word, signifies that nothing was done with the sorted data. No further analysis were done involving the shields nor the Ge crystals. Spectra produced with this method are commonly known as "singles" spectra.

Suppressed The "Suppressed" filter shows the germanium spectra when the ACS shields are used to suppress Compton scattered events.

Added back The "Added Back" filter utilizes the distance matrix in order to identify detections that may be results of Compton scattering within COMPEX detectors. For example, if there is a hit on a Ge crystal and another hit on a nearby crystal defined close enough by the distance matrix, the energies of the two hits are added in the spectrum. This process takes hits in different detectors caused by Compton scattering and ideally adds them to contribute to the photopeak.

Added back with suppression The "Added back with suppression" in essence combines the methods of Suppressed and Added Back. It does the selection for clean hits in the germanium crystals (no nearby ACS BGO hit) and also adds energy deposition in adjacent germanium detectors.

7 Results

The main data analysis was done by simulating an isotropic point-source of 661.7 keV gamma rays at the middle of the implantation detector. The 661.7 keV is the characteristic gamma radiation energy emitted by the decay of cesium-137. Cs-137 is commonly used in energy calibration as it has a single gamma emission energy from decaying barium-137. However the pure gamma ray source was used instead of decaying Cs-137 source to simplify the simulation by removing the decay process, as, for instance, the decay may proceed via internal conversion and complicate the analysis process. All the simulations were run with 10^6 events. The performances of the detectors were compared by calculating the peak-to-background ratio which was found by taking the ratio of the integral of the peak to the rest of the spectrum excluding the peak.

7.1 Lundium with ACS Response

A simulation was run with the Lundium setup including the ACS augmentation with the aforementioned isotropic point-like gamma ray source located at the middle of the implantation detector. This placement is effectively at the center of the decay station in the sense that each set of side detectors (COMPEX+BGOs) have the same solid angle coverage.

7.1.1 Verification through Hit Patterns

The validity of the simulation as well as the data sorting process can be confirmed by examining the hit patterns of the detectors. The hit patterns of the side and back detectors are inspected for verification. The hit patterns were generated in `Go4`.

Side Detectors Each of the detectors to the sides, germanium crystals in COMPEXs and BGOs alike, have varying degrees of solid angle coverage. Figure 11 illustrates the hit patterns of Ge crystals in a COMPEX and the accompanying BGO crystals. The coordinates of the two hit patterns in the figure are identical as indicated by similar pattern of hit counts of the two plots.

Looking at the hit patterns of the Ge crystals, one of them has clearly registered more hits with other crystals detecting less and less hits. This distribution is due to the solid angle coverage of the crystals in relation to the source. The differences in solid angle coverage can be clearly seen in the front view in Figure 10, where the location of the source is indicated with a small green dot on the implantation detector. Evidently, the Ge crystal closest to the detector has the largest angle coverage, followed by the crystal adjacent to it in the same plane (not protruding into the point of view).

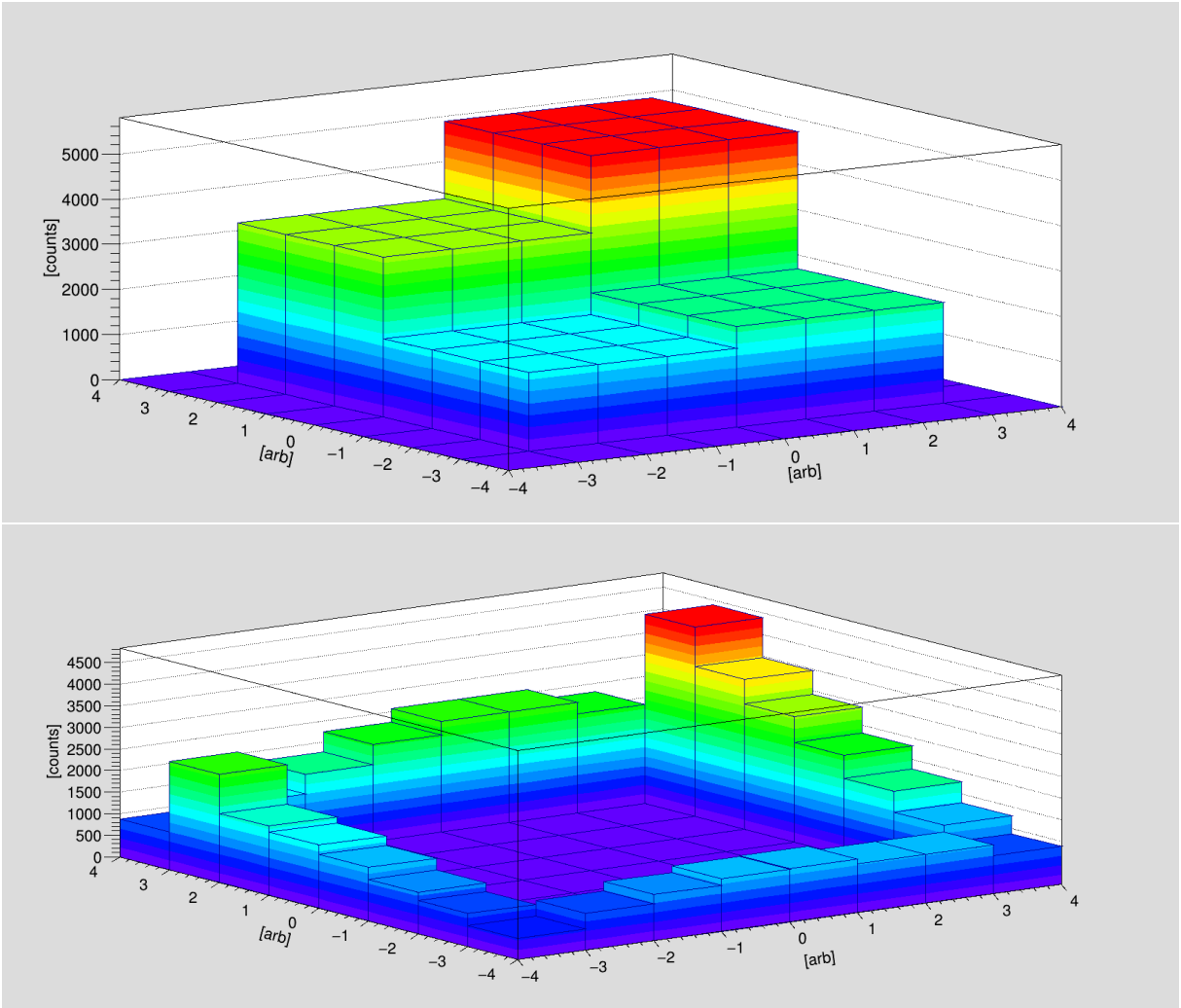

Figure 11: Hit patterns of a side COMPEX (top) and its ACS (bottom)

However, this crystal is partially shadowed by a crystal from the adjacent COMPEX detector. This overlap of the angle coverage leads to more hits on the overshadowing crystals that would have been registered in the shadowed crystal otherwise. The positions of the detectors and their corresponding hits were confirmed by cross-checking with detector ID numbers.

The solid angle coverage can also be seen through the similarities between the two plots

in Figure 11. The far back corner registers significantly more hits for both COMPEX and its ACS, providing a clear evidence of higher angle coverage. The hit patterns of all the side detector configurations (COMPEX + ACS) exhibit the same behavior as they are positioned symmetrically around the source.

Back Detectors Contrary to the side detectors, the back detectors display even distribution of hits, illustrated in Figure 12. Since the source is exactly in the middle of the COMPEX, this result is straightforward. The ACS exhibit a periodic behavior since the detectors around the silicon box are arranged symmetrically.

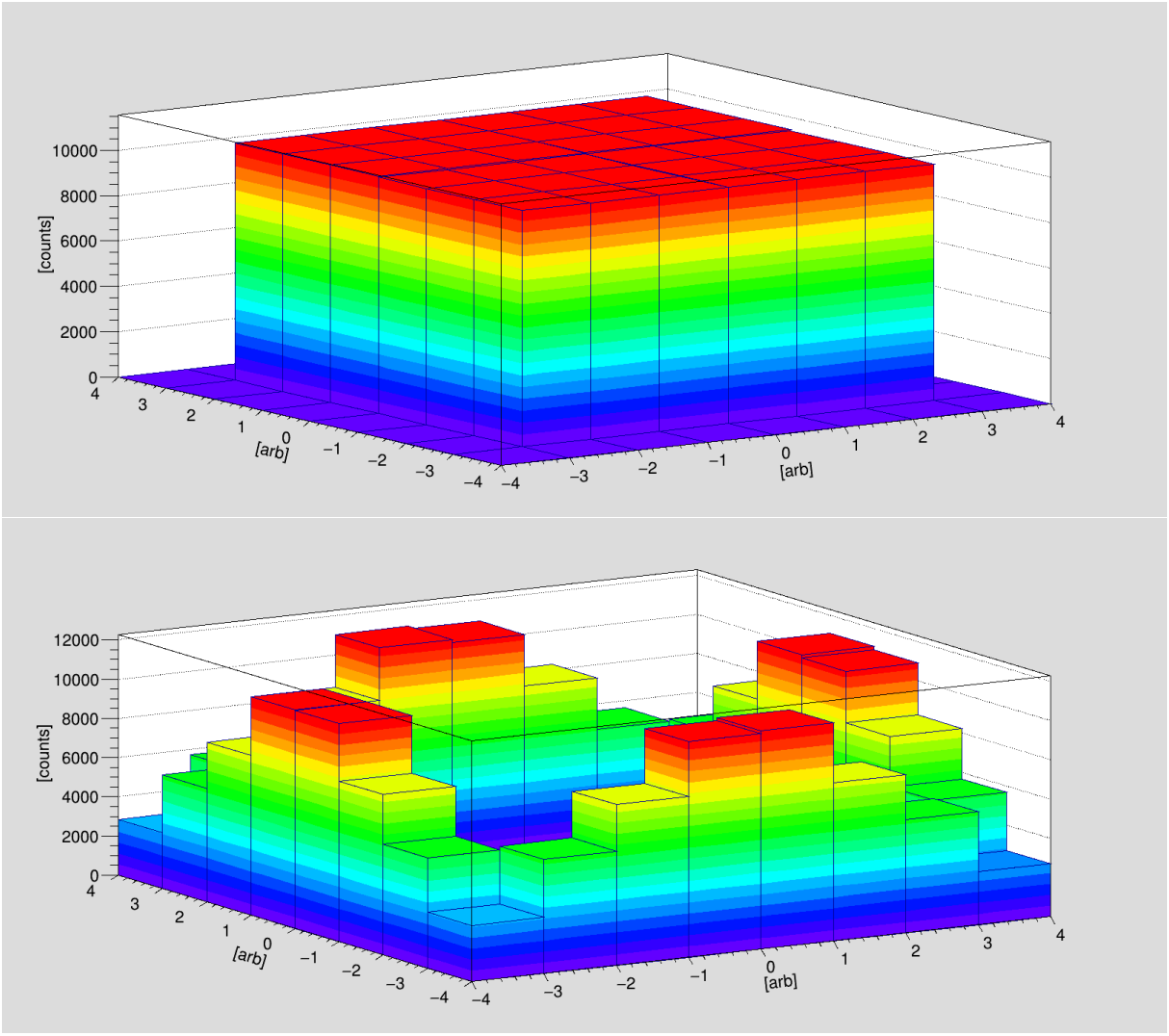

Figure 12: Hit patterns of a back COMPEX (top) and its ACS (bottom)

7.1.2 Performances of Data Filters

The simulated data from Lundium setup with ACS was filtered into the 4 categories. Each of the modified filters are compared with the Spectrum filter in Figure 13 in terms of their spectra, differences, and intensity ratios.

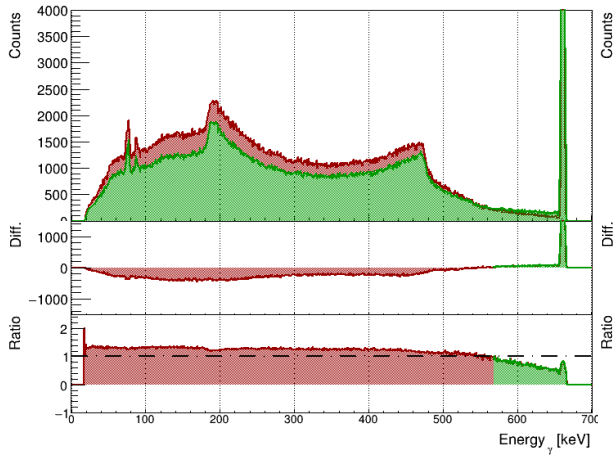

(a) Added Back

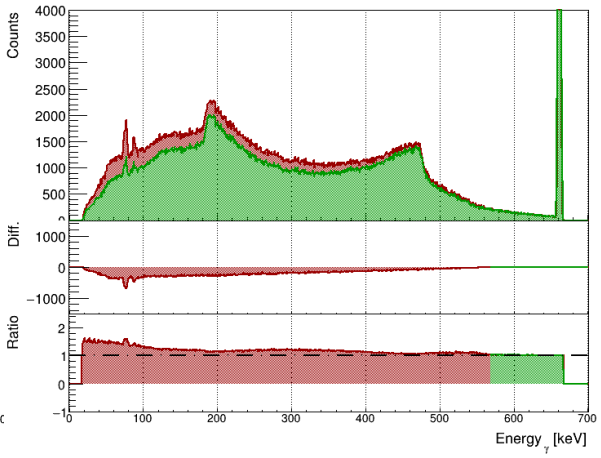

(b) Suppressed

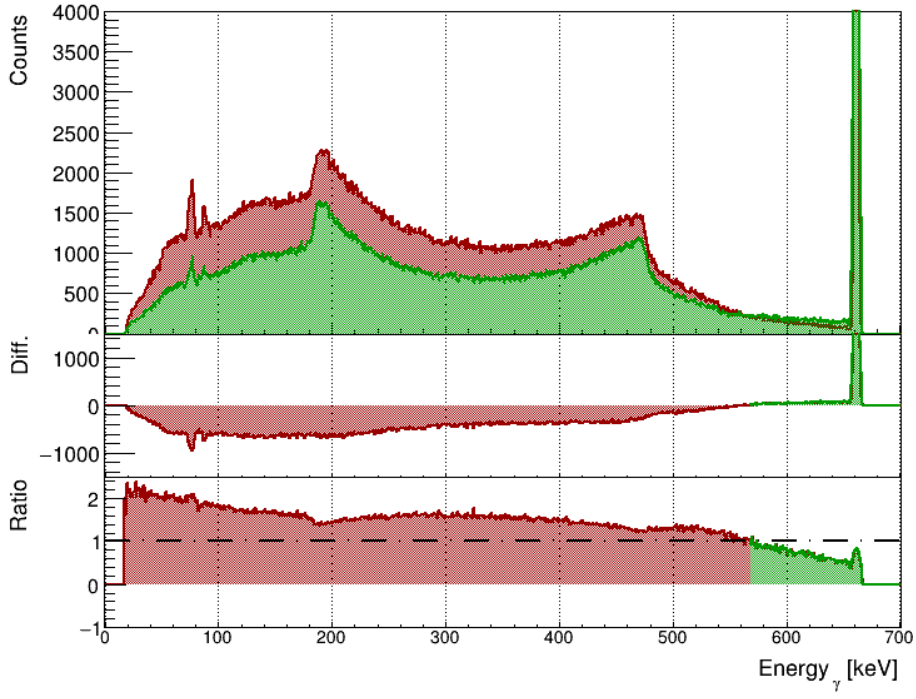

(c) Added back with suppression

Figure 13: Comparisons of spectra of filtered data from isotropic gamma source. Red spectra are the unfiltered "Spectrum" and green spectra are filtered with Added Back (left), Suppressed (middle), Added back with suppression (right). The top parts are direct comparisons of the spectra, and the middle portion shows the negative and positive differences in the spectra with corresponding colors for lesser and greater spectra. The bottom portion shows the ratio of the counts in the spectra, ranging from -1 to 1.

The effects of each filter can clearly be seen through their differences and their intensity ratios. The Added Back filter results in a higher photopeak intensity with slight reduction in background. The Suppressed results in much lower background than Added Back but unchanged photopeak intensity. However, with Added back with suppression, the background is greatly reduced, and the photopeak intensity is increased. The peak-to-background percentage of Spectrum is 25.5%. This measure increases with Suppressed, Added back, and Added back with suppression filters at 30.3%, 40.0%, and 49.0% re-

spectively to each filter. The peak-to-background percentages and the counts in the spectra and the peaks are shown in Table 1 in the Appendix. These increases in peak-to-background ratio indicates that the largest increase in detection performance is found using the Added back with suppression filter, also demonstrating the effectiveness of ACS.

7.2 Comparison of Lundium and ACS Augmented Lundium Setups

While comparing the different analyzed spectra gives insight into the validity of the data analysis, the value and the performance of the ACS can be ultimately found by comparing the spectra from the Lundium setup and the setup with ACS augmentation. This comparison directly shows the effects of suppression with the ACS as well as having the BGO crystals around the germanium detectors. Figure 14 shows the spectra, the difference between them, and the ratio of the responses from the two configurations. The red spectrum from Lundium is produced using the Added back process as Lundium setup does not have shields to consider. The green spectrum from Lundium with ACS is formed with Added back with suppression which demonstrates the best performance as detailed previously.

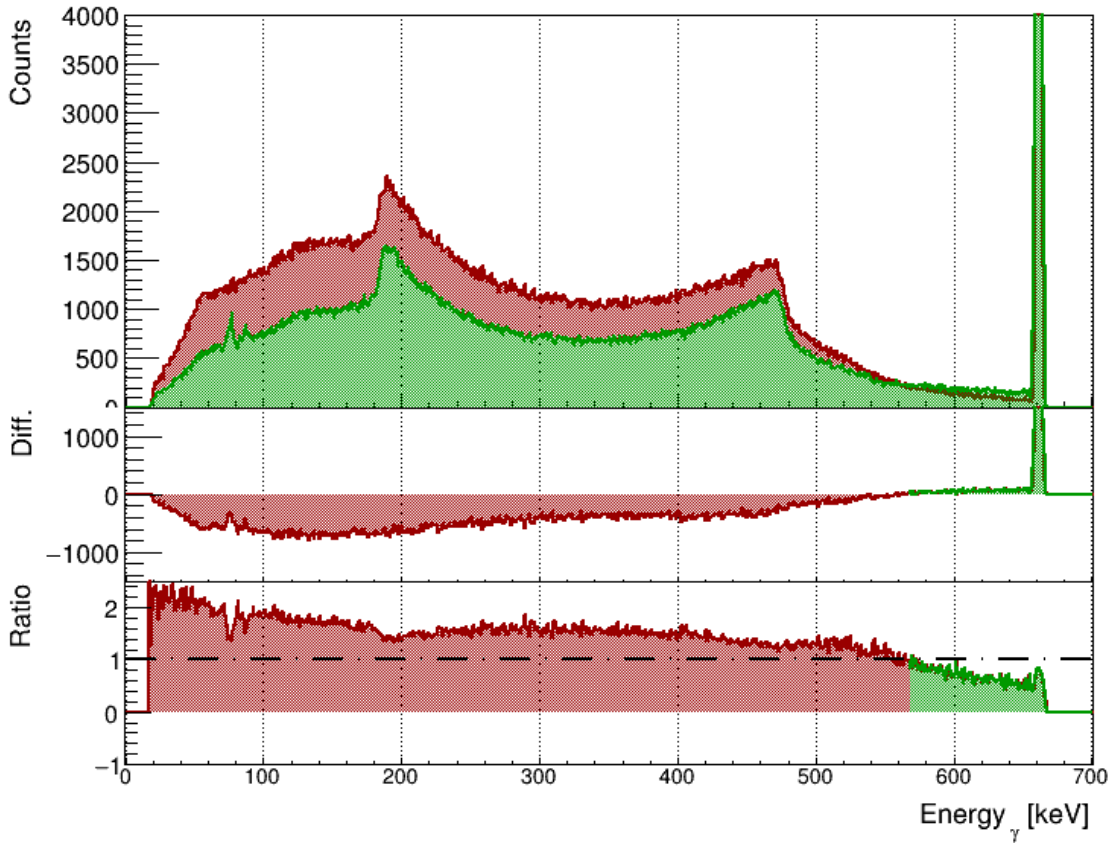

Figure 14: Simulated Response Comparison Between Lundium (red) and Lundium with ACS (green). Top portion shows direct comparison of the spectra. Middle portion shows the differences, and the bottom portion shows the ratios of the counts in the spectra.

The use of ACS significantly reduces the background intensities. However, the relative increase in the photopeak intensity is stunted in comparison. This can be additionally

seen by the peak-to-background measures with Lundium at 40.2% and Lundium with ACS yielding 49.0%, roughly only an increase of 9%. The simulated counts of the spectra and the peaks of these two runs are shown in Table 1 located in the Appendix. With the 9% increase in peak-to-background, implementation of the ACS provides a relative increase of 25%. Additional peaks from X-rays in the 70-80 keV range emitted by the surrounding BGOs can also be seen when utilizing the ACS.

7.3 Cs-137 Distributed on the Implant

While a point-source of a mono-energetic gamma ray is useful in comparing performances of different setups and filters, it does not completely reflect the typical experimental reality. To examine the shielding performance in a more realistic environment, the pure gamma ray source was replaced with a implanted Cs-137 ions with a Gaussian distribution that resembles the beam spatial distribution as shown in Figure 15. The implantation depth was achieved by implanting them with 35(5)MeV. This resembles the energy with which the ions leave TASCA into TASISpec. 10^6 events were simulated.

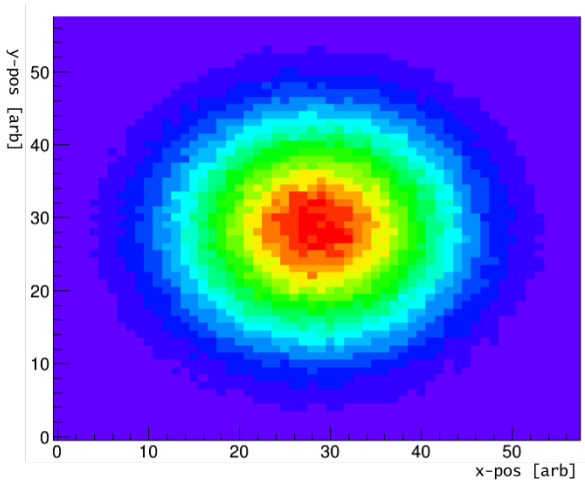

Figure 15: Distribution of Cs-137 on the implantation detector

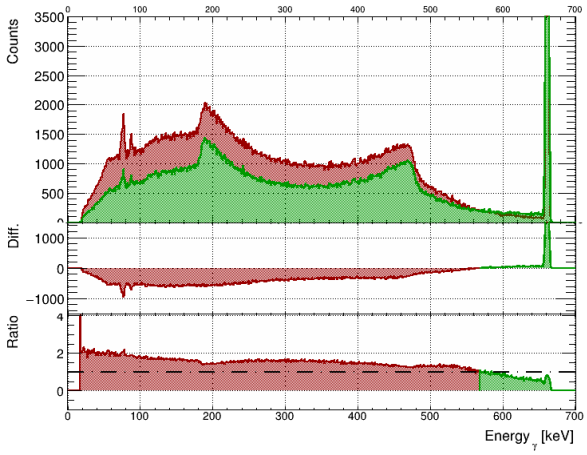

Figure 16: Simulated Response from Cs-137 Distribution in the Lundium setup with ACS (see Figure 15) with suppression (green) and without (red)

Comparisons were made between two filters of the data: Spectrum and Added back with suppression. The resulting spectra are shown in Figure 16. Similar to Figure 14, the background is significantly reduced, and the intensity of the photopeak is increased.

7.4 Effectiveness with Various Different Gamma Rays (Eu-152)

The effects of multiple gamma rays of different energies were also examined through the decay of Europium-152 [23]. The Eu-152 point-source was placed on the implantation detector and was simulated for 10^6 events as a point gamma source. Spectra from the Lundium setup with ACS are shown together in Figure 17 where black line shows the singles "Spectrum" and red shows "Added back with suppression" spectrum. As visible from the discrepancies of the intensities of the spectra, the filtering scheme used with the ACS also reduces the effects of Compton scattering in the detector for a more complicated emission.

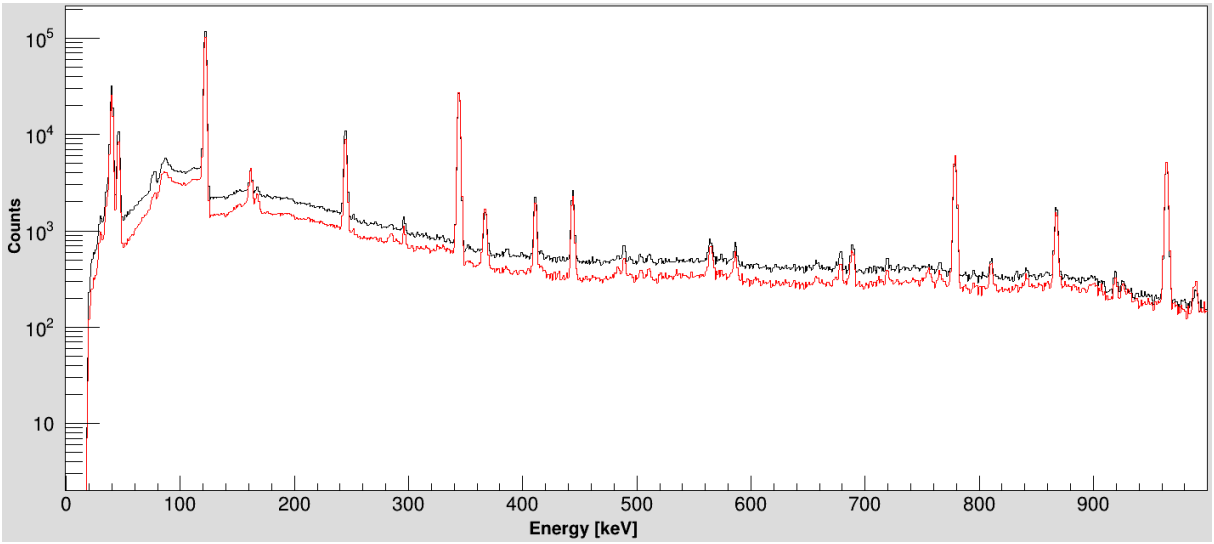

Figure 17: Simulated response from Eu-152 decay in the Lundium setup with ACS suppressed and added back (red) and singles spectrum (black).

8 Conclusion and Outlook

With data sorting and filtering verified to output and enhance data effectively to account for scattering events and the ACS, the augmentation to the Lundium decay station has yielded a 9% increase in peak-to-background percentage with this simulation. This yields a relative increase of 25% for this energy.

A more realistic simulation with distribution of Cs-137 resulted in similar behavior as the point-source, indicating that the performance of ACS with Lundium will be reliable in real experiments. The usage of ACS in the Lundium setup with multiple energies of photons with the filtering schemes has shown to reduce the Compton effects, yielding a increase in relative peak intensities. However, differently to a mono energetic source, it is difficult to determine a single metric to comprehensively compare the performances of these two setups due to the multiple number of peaks. Further analysis of specific peaks could yield insight into the effects of ACS for specific peaks or energy ranges.

The inclusion of ACS in the setup allows for more ways to process data, possibly increasing the peak-to-background ratio through a more suitable data filtering. The data analysis scheme for this simulation only takes into account the directly neighboring crystals from the same COMPEX detector as described in Section 6. However, this method could be extended to include the crystals from different detectors. For example, the same analysis with adding back with suppression can be done with a BGO bar from different COMPEX detectors as the ACS for a given COMPEX crystal. Since Compton scattering can occur without restrictions on direction excluding energetic restrictions, a photon may escape a BGO bar towards another BGO bar associated with another COMPEX. This extension of analysis could further reduce noise and improve relative peak intensity as energies escaping a COMPEX+ACS setup can still be accounted for.

Further simulations can be done to optimize positioning and geometry of the BGO crystals to maximize signal-to-background ratio by increasing the solid angle coverage. In addition, simulations involving low number of events can be done to examine the performance of the Lundium with ACS to mimic low number of events that occur with SHE experiments.

Acknowledgments

First and foremost, I would like to thank my supervisor Dr. Luis Sarmiento Pico for the opportunity to work on a project that taught me so much across so many things, answering my many questions with good insight, and the generous help with writing and technicalities of extending the Geant4 simulation. This thesis work has been possible and very enjoyable thanks to his expertise and the occasional fikas.

I would also like to thank Dr. Daniel Cox for the support and deepening my understanding of gamma spectroscopy as well as the help in writing and editing this thesis.

Finally, I'd like to thank my friend for the longest time, Jin Jang, for coming to Lund this semester, enriching my life in so many ways, and giving me brief but insightful view into C++ and object-oriented programming.

References

[1] Peter Moller and J Rayford Nix. "Stability of heavy and superheavy elements". In: *Journal of Physics G: Nuclear and Particle Physics* 20.11 (1994), p. 1681.

[2] Yuri Oganessian. "Nuclei in the" Island of Stability" of Superheavy Elements". In: *Journal of Physics: Conference Series*. Vol. 337. 1. IOP Publishing. 2012, p. 012005.

[3] R-D Herzberg et al. "Nuclear isomers in superheavy elements as stepping stones towards the island of stability". In: *Nature* 442.7105 (2006), p. 896.

[4] Dirk Rudolph et al. "Spectroscopy of element 115 decay chains". In: *Physical review letters* 111.11 (2013), p. 112502.

[5] Valeriy Zagrebaev, Alexander Karpov, and Walter Greiner. "Future of superheavy element research: Which nuclei could be synthesized within the next few years?" In: *Journal of Physics: Conference Series*. Vol. 420. 1. IOP Publishing. 2013, p. 012001.

[6] L-L Andersson et al. "TASISpec—A highly efficient multi-coincidence spectrometer for nuclear structure investigations of the heaviest nuclei". In: *Nuclear Instruments and Methods in Physics Research Section A: Accelerators, Spectrometers, Detectors and Associated Equipment* 622.1 (2010), pp. 164–170.

[7] L. G. Sarmiento. "Lundium Preparation Towards Flerovium [Spectroscopy]". May 2018.

[8] L. G. Sarmiento, L-.L. Andersson, and D. Rudolph. "A Geant4 simulation package for the TASISpec experimental detector setup". In: *Nuclear Instruments and Methods in Physics Research Section A: Accelerators, Spectrometers, Detectors and Associated Equipment* 667 (2012), pp. 26–31.

[9] Gordon Gilmore. *Practical gamma-ray spectroscopy*. John Wiley & Sons, 2011.

[10] Sea Agostinelli et al. "GEANT4—a simulation toolkit". In: *Nuclear instruments and methods in physics research section A: Accelerators, Spectrometers, Detectors and Associated Equipment* 506.3 (2003), pp. 250–303.

[11] Ch Lorenz et al. "Geant4-aided Quantum State Selective Decay Spectroscopy of 213Ra". In: *International Nuclear Physics Conference 2016*. Proceedings of Science. 2017, p. 073.

[12] Luis G Sarmiento. "Nuclear spectroscopy with Geant4-The superheavy challenge". In: *EPJ Web of Conferences*. Vol. 131. EDP Sciences. 2016, p. 05004.

[13] Kenneth S. Krane, David Halliday, et al. *Introductory nuclear physics*. 1987.

[14] Jan Verplancke et al. "Chapter 5 - Semiconductor Detectors". In: *Handbook of Radioactivity Analysis (Third Edition)*. Ed. by Michael F. L'Annunziata. Third Edition. Amsterdam: Academic Press, 2012, pp. 299–362. ISBN: 978-0-12-384873-4. DOI: https://doi.org/10.1016/B978-0-12-384873-4.00005-0. URL: http://www.sciencedirect.com/science/article/pii/B9780123848734000050.

[15] Glenn Frederick Knoll. *Radiation detection and measurement*. Wiley, 2000. ISBN: 0471073385.

[16] LL Andersson et al. "TASISpec–Heading towards its first experiment." In: ().

[17] Lisa Kirsebom. *Studying the world's heaviest elements*. accessed: May 05, 2019. 2016. URL: http://nucleardata.nuclear.lu.se/toi/index.asp.

[18] R Alba, G Bellia, and A Del Zoppo. "Performance of a symmetric BGO-NaI anti-compton shield". In: *Nuclear Instruments and Methods in Physics Research Section A: Accelerators, Spectrometers, Detectors and Associated Equipment* 271.3 (1988), pp. 553–556.

[19] KI Roulston and SIH Naqvi. "Reduced Compton effect scintillation spectrometer". In: *Review of Scientific Instruments* 27.10 (1956), pp. 830–832.

[20] Dirk P Kroese et al. "Why the Monte Carlo method is so important today". In: *Wiley Interdisciplinary Reviews: Computational Statistics* 6.6 (2014), pp. 386–392.

[21] Carlo Mancini Terracciano. *Monte Carlo methods and Geant4*. accessed: May 05, 2019. 2018. URL: `https://www.roma1.infn.it/~mancinit/Teaching/Trento/MCandGeant4Trento.pdf`.

[22] CERN. *ROOT*. URL: `https://root.cern/`.

[23] Richard B Firestone, LP Ekstrom, and SYF Chu. *WWW Table of Radioactive Isotopes*. 1998. URL: `http://nucleardata.nuclear.lu.se/toi/index.asp`.

9 Appendix

Table 1: Peak-to-background comparisons of different filters using Lundium and Lundium with ACS setups

Setup	**Filter**	**Total [counts]**	**Peak [counts]**	**Peak-to-background [%]**
Lundium	Added back	750922	215400	40.2
Lundium with ACS	Spectrum	834693	169700	25.5
Lundium with ACS	Suppressed	730103	169700	30.3
Lundium with ACS	Added back	750973	214600	40.0
Lundium with ACS	Added back with suppression	652875	214600	49.0